Adv. Polar Upper Atmos. Res., **20**, 27–37, 2006

Solar zenith angle and solar activity dependences of vertical profile of electron number density in the nightside auroral region

Atsushi Kumamoto*, Takayuki Ono and Masahide Iizima

Department of Geophysics, Tohoku University, Aoba, Aramaki, Aoba-ku, Sendai 980-8578
**Corresponding author. E-mail: kumamoto@stpp1.geophys.tohoku.ac.jp*

(Received December 22, 2005; Accepted April 3, 2006)

Abstract: Solar zenith angle and solar activity dependences of electron number density in the nightside auroral region from the topside ionosphere to the magnetosphere within a geocentric radial distance of 2.6 R_E were statistically investigated based on analysis of 7-years of plasma wave data measured by the plasma wave instrument onboard the Akebono (EXOS-D) satellite. The results are summarized as follows: (1) Electron number density N_e changes depending on solar zenith angle and solar activity: N_e in sunlight is about 3 times larger than that in darkness, and N_e during solar maximum is about 10 times larger than that during solar minimum. (2) During solar maximum, geopotential scale height is almost constant within a range from 250 km to 400 km. During solar minimum, geopotential scale height is drastically changes at a geopotential height around 2000–2500 km, or an actual height of 3000–4000 km: Geopotential scale height is 250–400 km below the transition height and larger than 500 km above the transition height. In order to discuss the auroral phenomena in various seasonal and solar activity conditions, the variations of ambient electron number density, as obviously shown in this study, should be taken into consideration in future studies.

key words: electron number density, nightside auroral region, seasonal variation, solar cycle variation, the Akebono (EXOS-D) satellite

1. Introduction

Ambient plasma density is a fundamental parameter for understanding auroral phenomena in the polar ionosphere and magnetosphere. The property of field-aligned currents and plasma waves in the polar region highly depends on the ambient plasma density. Electron number density (N_e) in the polar region has been observed by various methods: Sounder experiments (Hagg, 1967; Nelms and Lockwood, 1967; Timleck and Nelms, 1969; Benson and Calvert, 1979; Nsumei *et al*., 2003), wave measurements (Mozer *et al*., 1979; Benson and Calvert, 1979; Calvert, 1981; Persoon *et al*., 1983, 1988; Perraut *et al*., 1990), Langmiur probe measurements (Brace *et al*., 1970; Raitt, 1971; Mozer *et al*., 1979; Hilgers *et al*., 1992; Kletzing *et al*., 1998), and spacecraft potential measurements (Johnson *et al*., 2001; Janhunen *et al*., 2002). Early observations of N_e in the polar topside ionosphrere was performed by sounder onboard Allouette II (Hagg, 1967; Nelms and Lockwood, 1967; Timleck and Nelms, 1969) and probe measurements

onboard Exploler 22 and ESRO-1 (Brace *et al*., 1970; Raitt, 1971). From the sounder observations, it has been reported that N_e in the polar region is often below 100/cc. Based on ISIS-1 sounder measurement and Hawkeye wave measurement, extremely low N_e structure (less than 1/cc) has been found in an invariant latitude of $70\pm3^\circ$ from 1.8 R_E to 3 R_E and named "auroral plasma cavity" (Benson and Calvert, 1979; Calvert, 1981). It has also been confirmed that auroral plasma cavity is closely associated with auroral kilometric radiation sources (Benson and Calvert, 1979; Calvert, 1981; Perraut *et al*., 1990), precipitating electrons and upflowing ions (Persoon *et al*., 1988; Hilgers, 1992). Based on potential measurement of the Polar spacecraft, Janhunen *et al.* (2002) have shown that vertical extent of auroral plasma cavity depends on solar illumination condition at the magnetic foot point. Vertical profiles of N_e in the polar region were further investigated based on several spacecraft data. Mozer *et al.* (1979) derived vertical profile of N_e in the polar region from S3-3 Langmiur probe data and LHR wave data. Based on these measurements, an empirical model of N_e profile in the polar region has been developed, which is represented by combination of exponential and power functions (Lysak and Hudson, 1979; Kletzing and Torbert, 1994; Kletzing *et al*., 1998). Empirical power-law models of N_e profile have also been determined by DE-1 wave measurement (Persoon *et al*., 1983, 1988) and IMAGE sounder measurement (Nsumei *et al*., 2003).

Based on the statistical analyses of long-term satellite data, it has been reported that aurora-related phenomena, such as auroral electrons (Newell *et al*., 1996, 1998, 1999; Morooka and Mukai, 2003), upflowing ions (UFI) (Cattell *et al*., 1991; Collin *et al*., 1998; Morooka and Mukai, 2003), auroral kilometric radiation (AKR) (Kasaba *et al*., 1997; Kumamoto and Oya, 1998; Kumamoto *et al*., 2003a, b; Green *et al*., 2004), electromagnetic ion cyclotron (EMIC) waves (Elandson and Zanetti, 1998), and UV aurora intensity (Liou *et al*., 1997, 2001), show seasonal and solar activity dependences. As a possible controlling factor for these observed long-term variations, seasonal and solar cycle variations of ambient plasma density have been proposed.

In this study, N_e data in the nightside auroral region were derived from 7-years of plasma wave data obtained by the Akebono (EXOS-D) satellite, then statistically analyzed in order to clarify the seasonal and solar activity dependences of N_e in the nightside auroral region. In Section 2, derivation of N_e and methods of statistical analyses are described. In Section 3, N_e profiles obtained by statistical analyses and parameter fitting results are presented. Discussion and conclusions are given in Section 4.

2. Datasets and methods of analyses

Seven-years of plasma wave data obtained by the Plasma Waves and Sounder (PWS) instrument onboard the Akebono satellite were utilized for the statistical study of N_e in the nightside auroral region. The PWS instrument has been described in detail by Oya *et al.* (1990). The N_e was derived from upper limit frequency of whistler-mode auroral hiss. A typical Akebono PWS spectrogram with derived f_{pe} and N_e are shown in Fig. 1. In the invariant latitude larger than 60°, upper limit frequency of auroral hiss can be clearly identified around 100 kHz. The frequency is almost equal to plasma frequency f_{pe} in the polar region where plasma frequency f_{pe} is less than electron cyclotron

frequency f_{ce}. N_e is, then, determined by the f_{pe}, as shown in bottom panel of Fig. 1. It should be noted that the N_e in this study could be underestimated in cases where the wave normal direction of auroral hiss is oblique with respect to the magnetic field. As for the auroral hiss events analyzed in this study, the wave normal directions with respect to magnetic fields could not be confirmed due to the limitation of standard observation mode. Base on DE-1 wave measurements, it has been reported that auroral hiss propagates upward from a point source with spreading the ray path (Gurnett *et al*., 1983; Calvert and Hashimoto, 1990). However, as precisely discussed by Persoon *et al.* (1988), wave normal angle of auroral hiss with respect to the magnetic field tends to approach zero as the ray path approaches to $f=f_{pe}$ surface.

In order to focus on the nightside auroral region, the datasets obtained in the invariant latitude range from 65° to 75° in 2100 to 0300 magnetic local time (MLT) sector were selected for analyses in this study. In order to investigate seasonal and solar activity dependences of N_e the selected datasets were then divided into 4 subsets: (a) in sunlight during solar maximum, (b) in darkness during solar maximum, (c) in sunlight during solar minimum, and (d) in darkness during solar minimum. "In sunlight" and "in darkness" indicate solar zenith angle (SZA) conditions at the magnetic

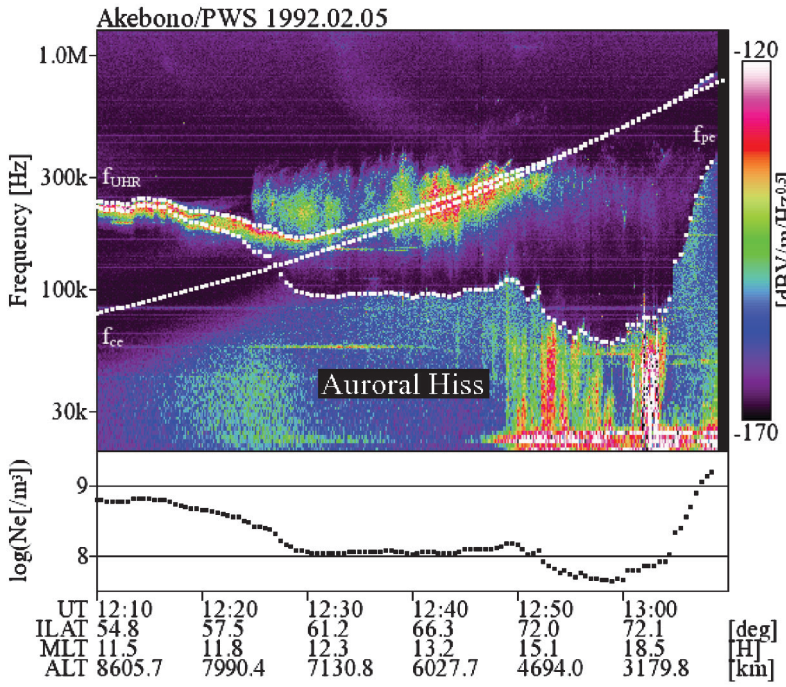

Fig. 1. An example of Akebono PWS spectrogram and derived N_e data. A typical spectrogram obtained by the Akebono PWS instrument is indicated in the upper panel. The electron cyclotron frequency (f_{ce}) derived from IGRF model, the plasma frequency (f_{pe}) and upper hybrid resonance (UHR) frequency (f_{UHR}) derived from whistler-mode auroral hiss and UHR wave spectra are also superposed in the upper panel with white dots. The N_e data calculated from the f_{pe} are indicated in the lower panel.

foot points in the polar ionosphere: "In sunlight" denotes $25^\circ < \mathrm{SZA} < 85^\circ$ and "in darkness" denotes $95^\circ < \mathrm{SZA} < 155^\circ$. The periods from April 1989 to March 1992, and from July 1993 to June 1997 are defined in this study as "solar maximum" and "solar minimum", respectively.

For each data subset, the average vertical profile of N_e was derived. In order to understand the obtained profiles by diffusive equilibrium model, geopotential height z was used as the height parameter. For given position, geopotential height z is defined as follows:

$$z = \int_{R_E}^{R_E+h} \frac{f_{\parallel}(r')}{g_0} dr', \tag{1}$$

where h is actual height of given position, g_0 is gravitational acceleration on the ground, and $f_{\parallel}$ is acceleration by gravity and centrifugal forces along the magnetic field. When the gravity force is not constant but proportional to $1/r^2$, the scale height $H = T/mf_{\parallel}$ depends not only on temperature T but also on r. On the other hand, the geopotential scale height $Z = T/mg_0$ depends only on temperature T.

3. Results

Figures 2 to 5 show scatter plots of N_e in the nightside auroral region in sunlight during solar maximum, in darkness during solar maximum, in sunlight during solar minimum, and in darkness during solar minimum, respectively. The lower and upper horizontal axes indicate geopotential height z and actual height h, respectively. The left and right vertical axes indicate N_e and corresponding plasma frequency f_{pe}. N_e profiles show clear solar zenith angle and solar activity dependences: N_e in sunlight or during solar maximum is larger than that in darkness or during solar minimum. N_e profiles in darkness are more scattered than those in sunlight. It can be also pointed out that N_e profiles during solar maximum shows almost constant gradient in all height range while N_e profiles during solar minimum changes their gradient at a transition height around $z = 2000$ km ($h = 3000$ km).

Geopotential scale heights Z in geopotential height ranges from $z = 300$ km to 1200 km, from 1300 km to 2200 km, and from 2300 km to 3200 km were determined by the least square fitting method with the following function:

$$\ln N_e = \ln N_{e0} - \frac{z - z_0}{Z}, \tag{2}$$

where z_0 is standard geopotential height, and N_{e0} is the electron number density at $z = z_0$. In this study, $z_0 = 1000$ km ($h = 1200$ km), $z_0 = 2000$ km ($h = 3000$ km) and $z_0 = 3000$ km ($h = 6000$ km) were respectively selected for fitting from $z = 300$ km to 1200 km, from 1300 km to 2200 km, and from 2300 km to 3200 km. N_e data above $z = 3200$ km ($h = 7000$ km) were not utilized for the fitting analysis in order to avoid unfavorable effects by the lower limit of N_e measurement range, which is due to the observation frequency range of the Akebono plasma wave data. Fitted lines are superposed on Figs. 2 to 5. Determined parameters are also summarized in Table 1. In order to compare the fitted N_e profiles, they are replotted in Fig. 6 with the empirical N_e model profile proposed by Kletzing *et al.* (1998) for reference. N_e in sunlight is about 3 times larger than that in darkness. N_e during solar maximum is about 10 times larger than that during solar

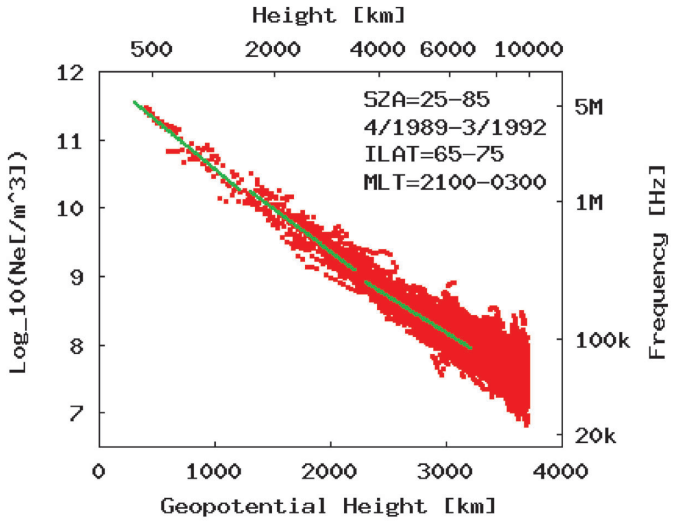

Fig. 2. Vertical distribution of electron number density N_e in sunlight during solar maximum (red dots). The lower and upper horizontal axes indicate geopotential height z and actual height h, respectively. The left and right vertical axes indicate electron number density N_e and corresponding plasma frequency f_{pe}. The fitted N_e profiles from z=300 km to 1200 km, from 1300 km to 2200 km, and from 2300 km to 3200 km are also indicated by green lines.

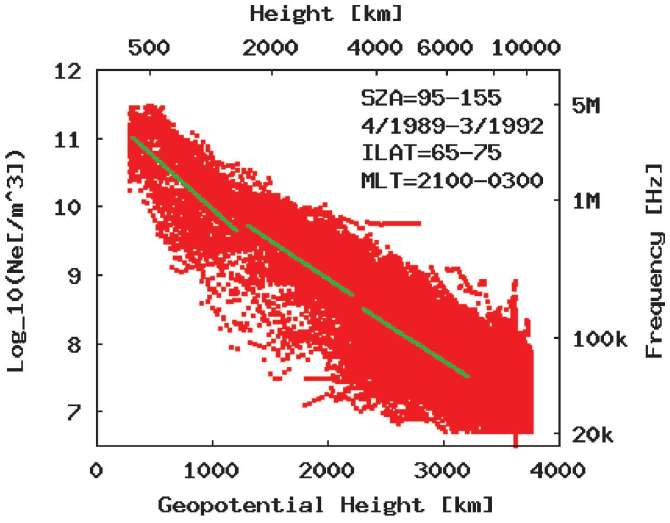

Fig. 3. Vertical distribution of electron number density N_e in darkness during solar maximum. The format is the same as Fig. 2.

minimum. During solar maximum, the geopotential scale height Z is around 250–400 km in all height range. During solar minimum, on the other hand, the geopotential scale height Z in the height range above z=2300 km becomes larger than 500 km in sunlight and 900 km in darkness. Geopotential scale height in each height range is

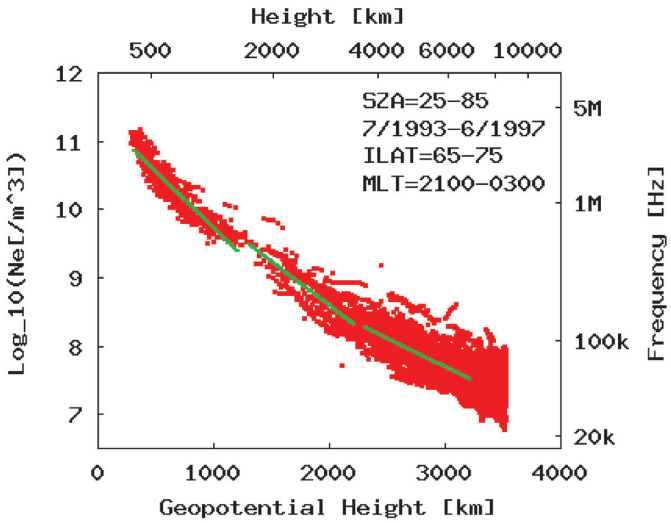

Fig. 4. Vertical distribution of electron number density N_e in sunlight during solar minimum. The format is the same as Fig. 2.

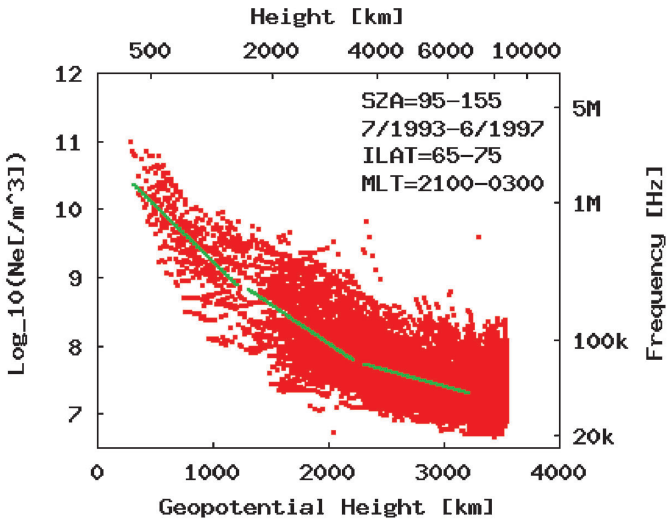

Fig. 5. Vertical distribution of electron number density N_e in darkness during solar minimum. The format is the same as Fig. 2.

Table 1. Electron number density at the standard height N_{e0} and geopotential scale height Z determined by the least square fitting method.

Solar activity	Solar zenith angle	Determined parameter					
		(z=300–1200 km)		(z=1300–2200 km)		(z=2300–3200 km)	
		N_{e0}[/m^3] (z_0=1000 km)	Z (km)	N_{e0}[/m^3] (z_0=2000 km)	Z (km)	N_{e0}[/m^3] (z_0=3000 km)	Z (km)
Maximum	25–85°	3.73×10^{10}	310	2.33×10^{9}	342	1.51×10^{8}	413
	95–155°	9.22×10^{9}	288	8.80×10^{8}	387	5.59×10^{7}	398
Minimum	25–85°	5.40×10^{9}	263	3.96×10^{8}	337	5.05×10^{7}	520
	95–155°	1.69×10^{9}	265	1.09×10^{8}	381	2.61×10^{7}	928

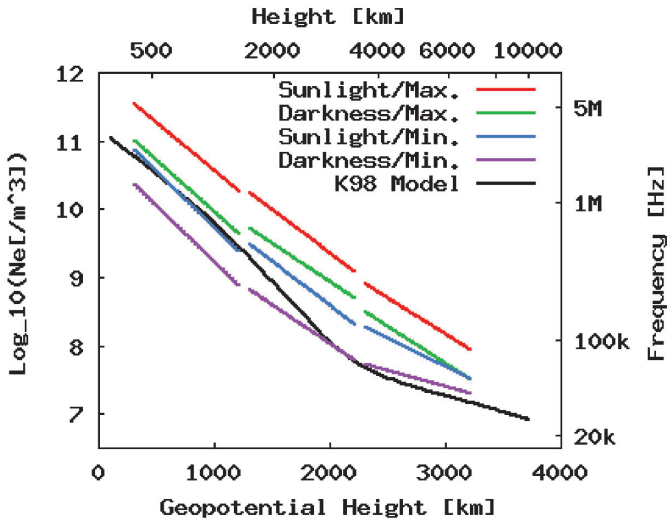

Fig. 6. The fitted N_e profiles in sunlight during solar maximum (red lines), in darkness during solar maximum (green lines), in sunlight during solar minimum (blue line), and in darkness during solar minimum (violet lines). The N_e profile of the empirical model proposed by Kletzing et al. (1998) is also indicated for reference (black curve).

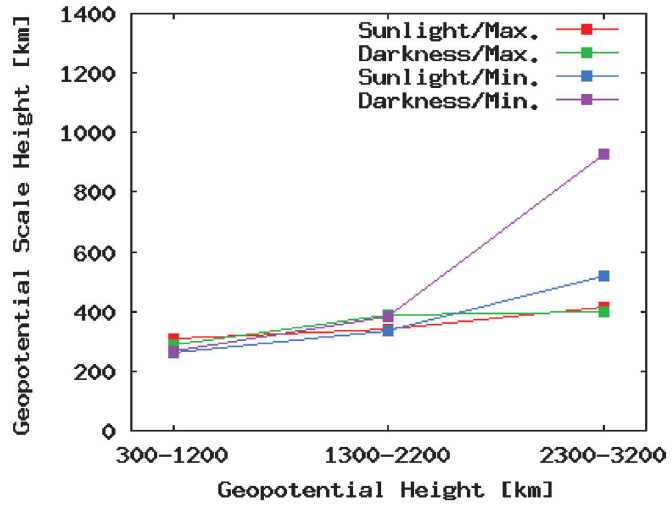

Fig. 7. Geopotential scale height determined by N_e profiles in sunlight during solar maximum (red lines), in darkness during solar maximum (green lines), in sunlight during solar minimum (blue line), and in darkness during solar minimum (violet lines).

plotted in Fig. 7. It can be clearly shown that geopotential scale height during solar minimum drastically changes between height ranges below 2200 km and above 2300 km.

4. Discussion and conclusions

Based on 7-years of plasma wave data obtained by the Akebono satellite, the solar zenith angle and solar activity dependences of N_e in the nightside auroral region within geocentric radial distance of 2.6 R_E are clarified as follows: (1) Electron number density N_e changes depending on solar zenith angle and solar activity: N_e in sunlight is about 3 times larger than that in darkness, and N_e during solar maximum is about 10 times larger than that during solar minimum. (2) During solar maximum, the geopotential scale height Z is almost constant: It is within a range from 250 km to 400 km. During solar minimum, the geopotential scale height Z drastically changes at a geopotential height around 2000–2500 km, or an actual height of 3000–4000 km: Geopotential scale height Z is 250–400 km below the transition height and larger than 500 km above the height.

As shown in Figs. 2 to 5, N_e profiles in darkness are more scattered than those in sunlight. It has been reported that auroral plasma cavity, which is probably associated with field aligned potential drops, often seen in the nightside auroral regions (Benson and Calvert, 1979; Calvert, 1981; Persoon *et al*., 1988). N_e profile in darkness could be a mixture of N_e profiles in the background and within the auroral plasma cavity.

The N_e profile during solar minimum is quite similar to the empirical model proposed by Kletzing *et al.* (1998). The coincidence is probably because the model is based on the S3-3 datasets obtained mainly in 1976, or during solar minimum. N_e profiles obtained in previous studies have also been summarized by Hilgers (1992). In Fig. 2 of Hilgers (1992), the N_e profile obtained by DE-1 is 3–10 times larger than that obtained by Viking. The DE-1 dataset was obtained in a period from 1981 to 1982 (Persoon *et al*., 1983), or during solar maximum. On the other hand, the Viking dataset was obtained in a period from 1986 to 1987, or during solar minimum. The difference of N_e, in these studies, is probably due to the solar activity dependence as determined in this study.

It is plausible that the electron components below the transition height are from the polar ionosphere. Because the ionization rate in the ionosphere highly depends on solar zenith angle and the solar EUV fluxes, they can affect the N_e profiles up to several thousand km height. Below the transition height, geopotential scale height Z is almost constant within 250–400 km, which suggests that ions and electrons probably distribute depending on diffusive equilibrium process with almost constant temperature. Kletzing *et al.* (1998) reported that electron temperature (T_e) is about 1 eV in an invariant latitude range from 65° to 80° below the altitude of 3000 km. Mean ion mass M is, therefore, the order of ten proton mass, which suggests that heavy ions such as O^+ are dominant below the transition height. Above the transition height, where light ions are dominant, it is also possible that N_e profile is mainly controlled by ion outflow process rather than diffusive equilibrium process. In this study, the transition height of geopotential scale height Z is found only during solar minimum. It is inferred that the transition height moves to a geocentric radial distance larger than 2.6 R_E during solar maximum. Assuming that (1) N_e profile of high-altitude plasma component, as seen above z=2300 km during solar minimum, does not change depending on solar zenith angle and solar activity conditions, and (2) geopotential scale height of low-altitude plasma component is almost constant not only below 2.6 R_E but also above 2.6 R_E, the

transition heights in sunlight and darkness during solar maximum are estimated to be z=4100 km (h=16000 km) and z=3600 km (h=9500 km), respectively.

N_e is one of the most important parameters in the polar region plasma. Seasonal and solar activity dependences of AKR have been clarified by some previous studies (Kumamoto *et al*., 2001, 2003a, b; Green *et al*., 2004). It should be pointed out that seasonal and solar cycle variations of N_e profile below the transition height seem to determine the vertical profile of AKR sources: Occurrence probability of AKR shows maximum at h=3500 km in winter (in darkness) during solar minimum, at h=4500 km in winter during solar maximum, at h=5500 km in summer (in sunlight) during solar minimum, and above 7000 km in summer during solar maximum. In all cases, N_e at these heights is about $10^8/m^3$. The N_e value is much larger than the criteria reported by the previous studies on AKR generation mechanism *via* cyclotron maser instability (CMI) processes (Benson and Calvert, 1979; Calvert, 1981; Lee *et al*., 1980; Hewitt *et al*., 1982). It is inferred that the dense cold plasma are locally depleted to be below 1/cc in the auroral field line by the field-aligned potential drops. The balanced N_e profile with cold plasma diffusions from the ionosphere and depletions by the field-aligned potential drops might determine the vertical profile of AKR sources. The N_e model proposed in this study is also useful for the derivation of vertical profile of Alfvén wave velocity including seasonal and solar activity effects. In previous theoretical and simulation studies on Alfvén waves in the polar region, "darkness/solar-minimum"-type N_e profile models are often used as a typical N_e profile. In order to discuss the auroral phenomena in various seasonal and solar activity conditions, the ambient N_e variations, as shown in this study, should be taken into consideration in future studies.

Acknowledgments

We would like to thank all the staff of the Akebono satellite team. This research was partly supported by the Grant-in-Aid for Young Scientists (B) 17740321, from The Ministry of Education, Culture, Sports, Science and Technology (MEXT), Japan.

The editor thanks Dr. J.L. Green and another referee for their help in evaluating this paper.

References

Benson, R.F and Calvert, W. (1979): ISIS-1 observations at the source of auroral kilometric radiation. Geophys. Res. Lett., **6**, 479–482.

Brace, L.H., Mayr, H.G. and Mahajan, K.K. (1970): A polar maximum of electron concentration at 1000 km altitude. J. Atmos. Terr. Phys., **32**, 1945–1957.

Calvert, W. (1981): The auroral plasma cavity. Geophys. Res. Lett., **8**, 919–921.

Calvert, W. and Hashimoto, K. (1990): The magnetoionic modes and propagation properties of auroral radio emissions. J. Geophys. Res., **95**, 3943–3957.

Cattell, C.A., Chari, S. and Temerin, M.A. (1991): An S3-3 satellite study of the effects of the solar cycle on the auroral acceleration process. J. Geophys. Res., **96**, 17903–17908.

Collin, H.L., Peterson, W.K., Lennartsson, O.W. and Drake, J.F. (1998): The seasonal variation of auroral ion beams. Geophys. Res. Lett., **25**, 4071–4074.

Elandson, R.E. and Zanetti, L.J. (1998): A statistical study of auroral electromagnetic ion cyclotron waves. J. Geophys. Res., **103**, 4627–4636.

Green, J.L., Boardsen, S., Garcia, L., Fung, S.F. and Reinisch, B.W. (2004): Seasonal and solar cycle dynamics of the auroral kilometric radiation source region. J. Geophys. Res., **109**, A05223, doi: 10.1029/2003JA010311.

Gurnett, D.A., Shawhan, S.D. and Shaw, R.R. (1983): Auroral hiss, Z mode radiation, and auroral kilometric radiation in the polar magnetosphere-DE 1 observations. J. Geophys. Res., **88**, 329–340.

Hagg, E.L. (1967): Electron densities of 8–100 electrons cm^{-3} deduced from Alouette II high-latitude ionograms. Can. J. Phys., **45**, 27–36.

Hewitt, R.G., Melrose, D.B. and Ronnmark, K.G. (1982): The loss-cone driven electron-cyclotron maser. Aust. J. Phys., **35**, 447–471.

Hilgers, A. (1992): The auroral radiating plasma cavities. Geophys. Res. Lett., **19**, 237–240.

Hilgers, A., Holback, B., Holmgren, G. and Bostrom, R. (1992): Probe measurements of low densities with applications to the auroral acceleration region and auroral kilometric radiation sources. J. Geophys. Res., **97**, 8631–8641.

Janhunen, P., Olsson, A. and Laakso, H. (2002): Altitude dependence of plasma density in the auroral zone. Ann. Geophys., **20**, 1743–1750.

Johnson, M.T., Wygant, J.R., Cattell, C., Mozer, F.S., Temerin, M. and Scudder, J. (2001): Observations of the seasonal dependence of the thermal plasma density in the Southern Hemisphere auroral zone and polar cap at 1 R_E. J. Geophys. Res., **106**, 19023–19033.

Kasaba, Y., Matsumoto, H., Hashimoto, K. and Anderson, R.R. (1997): The angular distribution of auroral kilometric radiation observed by the GEOTAIL spacecraft. Geophys. Res. Lett., **24**, 2483–2486.

Kletzing, C. and Torbert, R.B. (1994): Electron time dispersion. J. Geophys. Res., **99**, 2159–2172.

Kletzing, C.A., Mozer, F.S. and Torbert, R.B. (1998): Electron temperature and density at high latitude. J. Geophys. Res., **103**, 14837–14845.

Kumamoto, A. and Oya, H. (1998): Asymmetry of occurrence-frequency and intensity of AKR between summer polar region and winter polar region sources. Geophys. Res. Lett., **25**, 2369–2372.

Kumamoto, A., Ono, T. and Oya, H. (2001): Seasonal dependence of the vertical distributions of auroral kilometric radiation sources and auroral particle acceleration regions observed by the Akebono satellite. Adv. Polar Upper Atmos. Res., **15**, 32–42.

Kumamoto, A., Ono, T., Iizima, M. and Oya, H. (2003a): Seasonal and solar cycle variations of the vertical distribution of the occurrence probability of auroral kilometric radiation sources and of upflowing ion events. J. Geophys. Res., **108** (A1), 1032, doi: 10.1029/2002JA009522.

Kumamoto, A., Ono, T., Iizima, M. and Oya, H. (2003b): Control factor of solar cycle variation of auroral kilometric radiation. Adv. Polar Upper Atmos. Res., **17**, 48–59.

Lee, L.C., Kan, J.R. and Wu, C.S. (1980): Generation of auroral kilometric radiation and the structure of auroral acceleration region. Planet. Space Sci., **28**, 703–711.

Liou, K., Newell, P.T., Meng, C.-I., Brittnacher, M. and Parks, G. (1997): Synoptic auroral distribution: A survey using Polar ultraviolet imagery. J. Geophys. Res., **102**, 27197–27205.

Liou, K., Newell, P.T. and Meng, C.-I. (2001): Seasonal effects on auroral particle acceleration and precipitation. J. Geophys. Res., **106**, 5531–5542.

Lysak, R.L. and Hudson, M.K. (1979): Coherent anomalous resistivity in the region of electrostatic shocks. Geophys. Res. Lett., **6**, 661–663.

Morooka, M. and Mukai, T. (2003): Density as a controlling factor for seasonal and altitudinal variations of the auroral particle acceleration region. J. Geophys. Res., **108** (A7), 1306, doi: 10.1029/2002JA 009786.

Mozer, F.S., Cattel, C.A., Temerin, M., Torbert, R.B., Von Glinski, S., Woldorff, M. and Wygant, J. (1979): The DC and AC electric field, plasma density, plasma temperature, and field-aligned current experiments on the S3-3 satellite. J. Geophys. Res., **84**, 5875–5884.

Nelms, G.L. and Lockwood, G.E.K. (1967): Early results from the topside sounder in the Allouett II satellite. Space Research, VII, ed. by R.L. Smith-Rose. Amsterdam, North-Holland, 604–623.

Newell, P.T., Meng, C.-I. and Lyons, K.M. (1996): Suppression of discrete aurorae by sunlight. Nature, **381**, 766–767.

Newell, P.T., Meng, C.-I. and Wing, S. (1998): Relation to solar activity of intense aurorae in sunlight and darkness. Nature, **393**, 342–344.

Newell, P.T., Greenward, R.A. and Ruohoniemi, J.M. (1999): The role of the ionosphere in aurora and space weather. Rev. Geophys., **39**, 137–149.

Nsumei, P.A., Huang, X., Reinisch, B.W., Song, P., Vasyliunas, V.M., Green, J.L., Fung, S.F., Benson, R.F. and Gallagher, D.L. (2003): Electron density distribution over the northern polar region deduced from IMAGE/radio plasma imager sounding. J. Geophys. Res., **108** (A2), 1078, doi: 10.1029/2002 JA009616.

Oya, H., Morioka, A., Kobayashi, K., Iizima, M., Ono, T., Miyaoka, H., Okada, T. and Obara, T. (1990): Plasma wave observation and sounder experiments (PWS) using the Akebono (EXOS-D) satellite-Instrumentation and initial results including discovery of the high altitude equatorial plasma turbulence. J. Geomagn. Geoelectr., **42**, 411–442.

Persoon, A.M., Gurnett, D.A. and Shawhan, S.D. (1983): Polar cap electron densities from DE 1 plasma wave observations. J. Geophys. Res., **88**, 10123–10136.

Persoon, A.M., Gurnett, D.A., Peterson, W.K., Waite, J.H., Jr., Burch, J.L. and Green, J.L. (1988): Electron density deplections in the nightside auroral zone. J. Geophys. Res., **93**, 1871–1895.

Perraut, S, de Feraudy, H., Roux, A., Decreau, P.M.E. and Paris, J. (1990): Density measurements in key regions of the earth's magnetosphere-cusp and auroral region. J. Geophys. Res., **95**, 5997–6014.

Raitt, W.J. (1971): Polar ionospheric measurements from the ESRO-1 satellite. COSPAR Space Research, XI, Vol. 2, ed. by K.Ya. Kondratyev *et al.* Berlin, Akademie-Verlag, 1147–1161.

Timleck, P. and Nelms, G.L. (1969): Electron densities less than 100 electron cm^{-3} in the topside ionosphere. Proc. IEEE, **57**, 1164–1171.